Quantum Electronics **48** (3) 228–234 (2018)

NONLINEAR OPTICAL PHENOMENA https://doi.org/10.1070/QEL16528

Investigation of the dynamics of a nonlinear optical response in glassy chalcogenide semiconductors by the pump–probe method

E.A. Romanova, Yu.S. Kuzyutkina, V.S. Shiryaev, S. Guizard

Abstract. **An analysis of the results of measurements by using the pump–probe method with a femtosecond resolution in time and computer simulation of the charge carrier kinetics have revealed two types of a nonlinear optical response in samples of chalcogenide glasses belonging to the As–S–Se system, irradiated by 50-fs laser pulses with a wavelength of 0.79 μm. The difference in the nonlinear dynamics is due to the difference in the photoexcitation character, because laser radiation can be absorbed either through bound states in the band gap or without their participation, depending on the ratio of the pump photon energy to the bandgap energy.**

Keywords: *femtosecond laser pulses, photoinduced effects, optical nonlinearity, chalcogenide glasses, excitons.*

1. Introduction

Chalcogenide glasses (CGs), which are characterised by low optical loss in the wavelength range of 0.5–15 μm, good chemical stability, and high third-order optical nonlinearity, are promising materials for mid-IR optical data systems used in environmental monitoring, medical diagnostics, and online control of technological processes [1–3]. Since spectroscopic mid-IR sensors call for both sensor elements and compact broadband sources of coherent radiation, CG processing techniques should be developed. Femtosecond laser modification (FLM) technology [4–6] can be used to form waveguide structures on the surface of CGs and in their bulk. However, the chemical and physical effects leading to a change in the optical properties of CGs under high-intensity femtosecond laser pulses have been scarcely studied. To develop FLM technology as applied to CGs, one needs fundamental knowledge about the photoinduced processes occurring in glasses of different compositions. The study of the nonlinear optical response in CG samples is important for the following reason: FLM technology is in essence nonlinear, because the pulse propagation conditions and pulse energy absorption in a glass sample depend on the values of the Kerr constant and multiphoton absorption coefficient for this glass [7].

Currently, there is no rigorous theory describing the nonlinear optical response in topologically disordered structures, in particular, in glassy semiconductors, to which CGs belong. In some works, the nonlinear optical coefficients of CGs were estimated using the predictions of the theory of nonlinear optical response in crystalline semiconductors [8–10]. At the same time, systemised empirical studies revealed a relationship between the composition, structure, and nonlinear optical properties for some CG systems [2, 11–14]. These studies include both measurements of nonlinear optical coefficients (Kerr constant, multiphoton absorption coefficient, Raman-amplification coefficient) and structural analysis of glasses by methods of Raman scattering, Fourier spectroscopy, X-ray spectroscopy, X-ray diffraction analysis, and nuclear magnetic resonance spectroscopy. It was established that, since the interatomic bonds in CGs are weaker than in oxide glasses, the band gap in CGs is generally narrower than 3 eV, and the glass-transition temperature $T_g < 200\,^{\circ}C$. At the same time, the density ($3.2–5.0\ g\ cm^{-3}$) and refractive index (2.3–3.4) of CGs are much higher than those for oxide glasses. The Kerr constant for CGs is 2 to 3 orders of magnitude larger than the Kerr constant for quartz glass.

To optimise FLM technology, it is important to investigate the temporal character of the photoinduced processes leading to changes in the refractive index of glass. Previously, we studied the temporal dynamics of nonlinear optical response in glasses of the As–S–Se system by the pump–probe method [15] with a femtosecond resolution in time. The nonlinear optical coefficients of refraction and absorption were determined in [10] at relatively low pump pulse intensities, when the density of photoinduced charge carriers can be neglected. The results of measurements at high pump intensities showed [16, 17] that the character of the nonlinear response (including the carrier kinetics) on time intervals up to 10 ps depends on the proximity of the laser pulse frequency to the fundamental absorption band edge of the CGs under study.

In this study, based on analysis of the experimental results obtained at high pump intensities, we developed theoretical models of charge carrier kinetics in glasses belonging to the As–S–Se system and performed computer simulation of the nonlinear response dynamics. Matching of the calculated and measured dependences made it possible to determine the parameters characterising the electronic properties of the glasses under consideration. We also briefly described the structural features of the glasses of this system and assigned the character of their charge carrier kinetics to possible photoinduced changes in the glass molecular network.

E.A. Romanova, Yu.S. Kuzyutkina N.G. Chernyshevsky Saratov State University, ul. Astrakhanskaya 83, 410012 Saratov, Russia; e-mail: elena_rmnv@yahoo.co.uk, romanova@optics.sgu.ru;
V.S. Shiryaev G.G. Devyatykh Institute of Chemistry of High-Purity Substances, Russian Academy of Sciences, ul. Tropinina 49, 603600 Nizhny Novgorod, Russia; e-mail: shiryaev@ihps.nnov.ru;
S. Guizard Ecole Polytechnique, 91128, Palaiseau, France

Received 5 October 2017; revision received 14 November 2017
Kvantovaya Elektronika **48** (3) 228–234 (2018)
Translated by Yu.P. Sin'kov

2. Chalcogenide glasses of the As–S–Se system

The structure of glasses of stoichiometric compositions, $As_{40}S_{60-x}Se_x$, has been thoroughly investigated using different experimental techniques [1, 2, 11–14, 18–20]. The molecular bonds in this system are mainly covalent. X-ray diffraction analysis showed that the glass structure is formed by corrugated layers; the degree of corrugation increases with increasing chalcogen atom size. Trigonal pyramids [AsS_3] and [$AsSe_3$] with an arsenic atom in the vertex, which are linked via doubly coordinated chalcogen, are distinguished in the structure of As_2S_3 and As_2Se_3 glasses. A partial substitution, for example, of selenium for sulphur in As_2S_3 glass gives rise to mixed-type [$As(S,Se)_3$] pyramids. In particular, it was demonstrated in [21] that [$AsSSe_2$] and [AsS_2Se] heteropyramids and [AsS_3] and [$AsSe_3$] homopyramids may coexist in the amorphous $As_{40}S_{60-x}Se_x$ system. Studies using nuclear magnetic resonance spectroscopy and Raman scattering showed [11] that S and Se atoms in this system are uniformly distributed throughout the glass volume when the concentration of Se atoms is equal to the sulfur concentration or exceeds it. At lower Se concentrations, chalcogens atoms form clusters.

Under illumination, the electronic polarisability of Se atom exceeds that of S atom, because the valence electrons in the heavier Se atom are more weakly bound with the nucleus. Therefore, a partial replacement of sulphur with selenium increases the electronic susceptibility of the medium and its refractive index in the range of normal glass dispersion. CGs always have homopolar bonds; however, the concentration of these bonds is minimum in a stoichiometric composition. In the case of partial replacement of sulphur with selenium, the formation of mixed-type pyramids is accompanied by the occurrence of Se–Se and S–S bonds and violation of the glass structure lamination, which is believed to be another factor enhancing the nonlinear optical response [14].

Note that the values of glass optical parameters are determined by the degree of connectivity of molecular network sites, whereas the other macroscopic characteristics (density, glass-transition temperature, coefficient of thermal expansion) are controlled by the connectivity of structural units [$As(Ch)_3$]; the dependence of these parameters on the Se concentration in $As_{40}S_{60-x}Se_x$ glasses is linear. The dependence of the optical band gap E_g on the Se concentration is also close to linear.

According to the Moss rule [2], far from the fundamental absorption edge, the refractive index of amorphous semiconductors increases with a decrease in E_g. Correspondingly, the Kerr constant n_2 increases as well. Concerning the CG system under consideration, this specificity of the electronic and optical properties is due to the weakening of interatomic bonds at partial replacement of sulfur with selenium and the change in the ratio of energies of all covalent bonds: As–S, As–Se, and S–Se.

To study the photoinduced processes in noncrystalline semiconductors, it is necessary to take into account the exciton energy bands (formed by bound states in the band gap), which are due to the absence of long-range order in the glass molecular network. The bound states in CGs correspond to such structural features as homopolar and dangling bonds and lone pairs of p electrons on the outer shell of chalcogen atoms [1, 2]. Since the electron–phonon interaction is strong in CGs [18], these bound states can be attributed to self-trapped excitons. Due to the presence of exciton bands, the fundamental absorption edge of CGs has a region of exponential decrease in the absorption coefficient α (Urbach tail), which passes to a weak absorption tail ($\alpha < 1$ cm^{-1}).

The weak connectivity of glass network and the existence of lone pair electrons, whose energy states lie in the top of the valence band, determine the specificity of photoinduced processes in CGs, in particular the photodarkening effect [2], where changes in the molecular glass network narrow the band gap and change the refractive index in the illuminated region.

3. Measurement technique and results

The nonlinear optical response in CG compositions was investigated using a Ti:sapphire laser, generating pulses with FWHM $\tau = 50$ fs and peak wavelength $\lambda_0 = 0.79$ μm, as a light source. An optical scheme of the setup [10] is presented in Fig. 1.

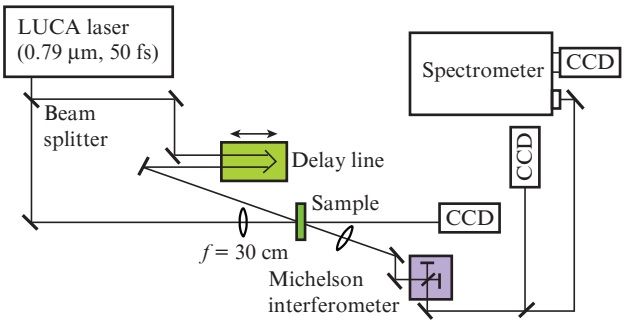

Figure 1. Optical scheme of the setup for studying the nonlinear optical response by three-pulse pump–probe interferometry.

The compositions of the glass samples of the $As_{40}S_{60-x}Se_x$ system were chosen so as to make the pump centre frequency ν_0 fall in the weak absorption tail ($x = 0, 15, 20, 30$) or Urbach tail ($x = 40, 45, 60$). The corresponding values $R = h\nu_0/E_g$ are listed in Table 1. Glass samples in the form of thin disks of different thicknesses ($d = 0.5–1.2$ mm) were prepared according to the standard technique by melting raw materials in a quartz glass ampoule. The samples were polished from both sides to surface finish of 0.25 μm (the sample preparation technology was described in detail in [10, 22]).

The pump pulse energy in the experiments was varied within 0.2–12 μJ. To exclude the cumulative effect, samples were moved during the experiment so as to expose each point of the sample surface to only one pump pulse.

Numerical values of the phase shift $\Delta\varphi$ and probe pulse absorptance were recorded in the form of a matrix in the entire range of probe pulse time delays Δt with respect to the pump pulse, with a specified time interval, and at the 'points' of probe beam cross section, whose sizes (3.6 μm) are determined by the pixel size in the CCD camera. The phase shift and absorptance values, averaged over the beam cross section in the entire range of Δt, were recorded in a separate file.

An analysis of the nonlinear response in the samples under study revealed two different types of temporal dynamics. For the glass compositions with $x = 0$, 15, and 20, the intersection points of the curves $\Delta\varphi(\Delta t)$ with the abscissa axis are determined by the pump pulse energy. The dynamics of this type is shown in Fig. 2a by an example of the $As_{40}S_{60}$ sample, for

Table 1. Main characteristics of glasses of the $As_{40}S_{60-x}Se_x$ system.

Glass composition	Density/g cm^{-3}	Refractive index n_0 ($\lambda_0 = 0.79$ μm)	Glass-transition temperature T_g/°C	Optical band gap E_g/eV	$R = h\nu_0/E_g$
$As_{40}S_{60}$	3.20	2.52	215	2.35	0.66
$As_{40}S_{45}Se_{15}$	3.56	2.65	207	2.20	0.71
$As_{40}S_{30}Se_{30}$	3.92	2.80	202	2.0	0.78
$As_{40}S_{15}Se_{45}$	4.27	2.95	196	1.90	0.82
$As_{40}Se_{60}$	4.59	3.02	191	1.75	0.90

which the pump photon energy $h\nu_0$ corresponds to the red edge of weak absorption tail ($R = 0.66$; Table 1), $\alpha_0 = 0.1$ cm^{-1}. For each of the compositions with x = 30, 40, and 45, the curves $\Delta\varphi(\Delta t)$ intersect the abscissa axis at the same time delay, independent of the pump pulse energy E, as shown for the $As_{40}S_{30}Se_{30}$ sample in Fig. 2b. The energy $h\nu_0$ for this sample lies in the weak absorption tail near the Urbach tail red edge ($R = 0.78$; Table 1), $\alpha_0 = 0.4$ cm^{-1}.

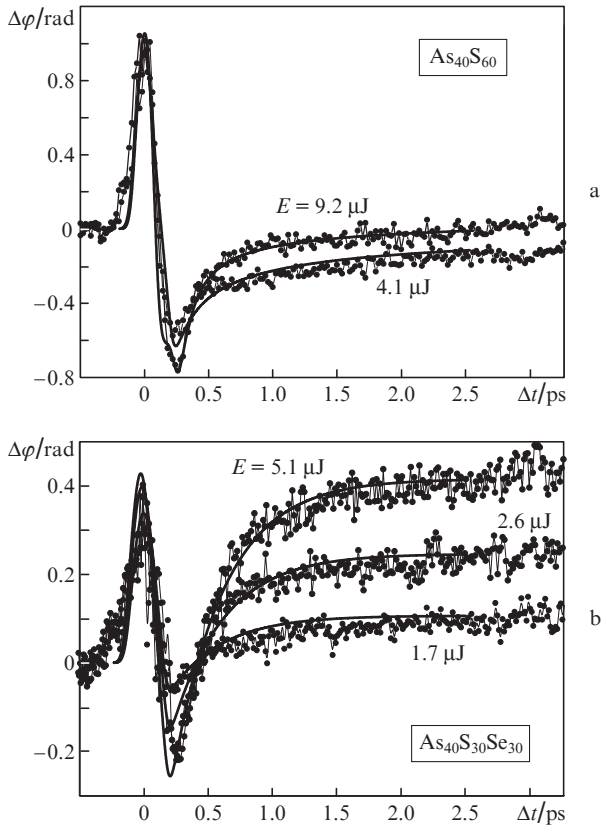

Figure 2. Dependences of the probe pulse phase shift, averaged over the transverse beam profile, on the probe pulse time delay with respect to the pump pulse for the (a) $As_{40}S_{60}$ and (b) $As_{40}Se_{30}S_{30}$ samples at different pump pulse energies E (circles are measured values, solid lines are calculation results).

The E values in Fig. 2 correspond to the following pump peak intensities I_0 on the front surface of the $As_{40}S_{60}$ sample: 450 GW cm^{-2} ($E = 4.1$ μJ) and 1 TW cm^{-2} ($E = 9.2$ μJ); for the $As_{40}Se_{30}S_{30}$ sample, the peak intensities are 125 GW cm^{-2} (E = 1.7 μJ), 190 GW cm^{-2} (E = 2.6 μJ), and 380 GW cm^{-2} (E = 5.1 μJ). The pump pulse intensity was determined from the formula $I_0 = E_{in}/(\tau S)$, where E_{in} is the pump pulse energy with allowance for the Fresnel reflection from the sample surface and $S = \pi w^2$. The pump beam radius w was found from the profile of the probe beam phase shift in the pump beam cross section at small E values.

As can be seen in Fig. 2, a characteristic peak arises in the curves in the vicinity of $\Delta t \approx 0$ due to the cross-phase modulation of the probe pulse when the latter is overlapped with the pump pulse. The transition of $\Delta\varphi(\Delta t)$ to the domain of negative values is indicative of an increase in the electron density in the conduction band. Then $\Delta\varphi$ decreases in modulus to zero due to charge carrier recombination. The time delay at which $\Delta\varphi = 0$ characterises the transition time Δt_0 of charge carriers to bound states in the band gap. For the $As_{40}S_{60}$ composition, the Δt_0 value depends on E. A similar dynamics was observed in a crystalline NaCl sample in [15]; it was explained by the occurrence of hole self-trapping immediately after the charge separation. A free electron could move in the sample during some time until it formed a bound state with a hole (self-trapped exciton). Excitons are formed more rapidly with an increase in E because of the higher density of electron–hole pairs.

In contrast, the Δt_0 value for the $As_{40}Se_{30}S_{30}$ samples was found to be independent of E. A similar temporal dynamics of nonlinear response was observed in [15] for crystalline quartz; it was explained by the direct transition of charge carriers to exciton states after photoexcitation.

Here, we used the data on the charge carrier kinetics from [15] to analyse the photoinduced processes in CG samples. The type of a photoinduced process (single- or multiphoton) can be determined by plotting a dependence of the phase shift $\Delta\varphi_{min}(I_0)$ in the minimum of curve $\Delta\varphi(\Delta t)$. This dependence (Fig. 3, circles) is approximated well by a quadratic function for both samples, a circumstance suggesting a dominant role of two-photon processes in carrier photoexcitation. The change in the character of the dependence at large I_0 values corresponds to the functional dependence of radiation intensity in the case of two-photon absorption: $I(I_0) = I_0/(1 + I_0\beta_2 z)$.

Let us now consider the dependence of the phase shift $\Delta\varphi_c$ on I_0 at long delay times ($\Delta t > 100$ ps), when the $\Delta\varphi_c$ value is independent of Δt. For the $As_{40}S_{60}$ sample, the dependence $\Delta\varphi_c(I_0)$ at pump pulse intensities ranging from 350 to 700 GW cm^{-2} is also quadratic, whereas for the $As_{40}S_{30}Se_{30}$ sample this dependence is close to linear (Fig. 3, triangles). Note that, at $I_0 < 300$ GW cm^{-2}, the transition of $\Delta\varphi$ to the domain of positive values is not observed for the $As_{40}S_{60}$ sample up to $\Delta t \approx 1$ ns; this fact indicates that either there is an intensity threshold for the observed photoinduced changes or these changes occur very slowly. The linear dependence $\Delta\varphi_c(I_0)$ for the $As_{40}S_{30}Se_{30}$ sample indicates that excitons arise as a result of single-photon process, because two-photon absorption may occur via energy levels in the band gap; i.e., it is a two-step process.

An analysis of the time dependences of absorptance [17] indicates that there is residual absorption in a sample at long probe delay times.

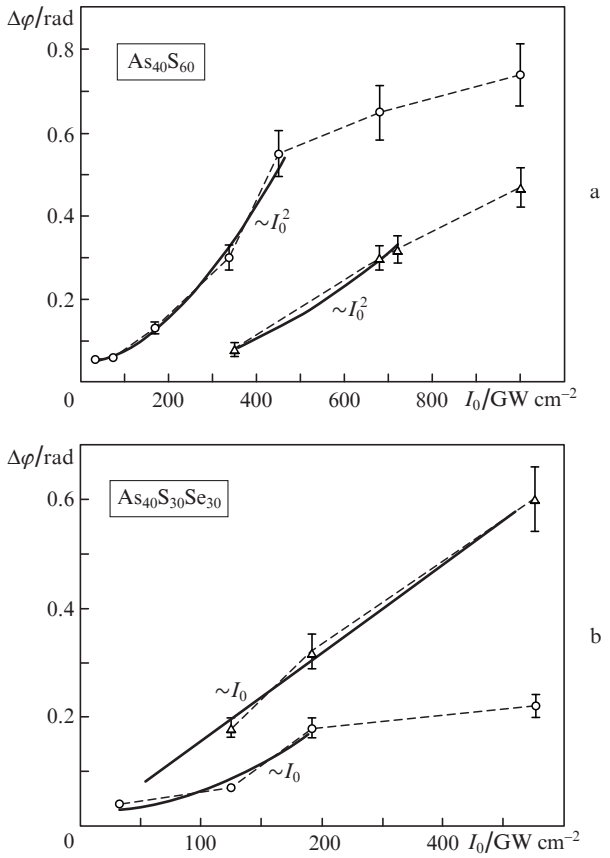

Figure 3. Dependences of the absolute value of probe pulse phase shift on the pump peak intensity (○) in the minimum of the dependence $\Delta\varphi(\Delta t)$ and (△) in the range $\Delta t > 100$ ps for the (a) $As_{40}S_{60}$ and (b) $As_{40}S_{30}Se_{30}$ samples.

4. Computer simulation of the nonlinear optical response dynamics

The change (averaged over the beam cross section) in the phase φ_2 of a probe pulse propagating in a sample in the z direction is determined from the equation

$$\frac{\partial\varphi_2(t,z)}{\partial z} = k_0\Delta n(t,z), \tag{1}$$

where $k_0 = 2\pi/\lambda_0$. The following expression was obtained for the photoinduced change in the refractive index in [15] in the plane-wave approximation:

$$\Delta n \approx pn_2I_1 + \frac{e^2}{2n_0\varepsilon_0}\left[-\frac{N_e f_{CB}}{m^*\omega^2} + \frac{N_{te}f_{tr}}{m(\omega_{tr}^2-\omega^2)}\right]. \tag{2}$$

Here, the coefficient p is 1 or 2 if the planes of polarisation of the pump and probe pulses are perpendicular or parallel, respectively; n_2 is the Kerr constant; I_1 is the pump pulse intensity; n_0 is the refractive index of the material; ε_0 is the permittivity of free space; e, m, and m^* are, respectively, the charge, electron mass, and electron effective mass in the conduction band; f_{CB} and f_{tr} are the oscillator strengths for the transitions from the valence band to the conduction and exciton bands, respectively; ω is the laser frequency; ω_{tr} is the exciton transition frequency; N_e is the free-electron density; and N_{te} is the exciton density.

Expression (2) was derived in [15] on the assumption that the contribution of holes to Δn can be neglected and the density of excited electrons is low in comparison with the electron density in the valence band. The first term in the right-hand side of (2) corresponds to the effect of probe pulse cross-phase modulation. The two terms in square brackets describe the change in the refractive index due to the charge separation: the first, proportional to the conduction electron density, is always negative, while the second, proportional to the exciton density, is positive if $\omega_{tr} > \omega$.

The decrease in the pump beam intensity in the sample is mainly due to the one- and two-photon absorption in the glass and to the Joule loss (beam energy absorption by free electrons):

$$\frac{\partial I_1(t,z)}{\partial z} = -[\alpha_1 + \beta_2 I_1(t,z) + \gamma_e n_e(t,z)]I_1(t,z), \tag{3}$$

where α_1 and β_2 are the one- and two-photon absorption coefficients, respectively; $\gamma_e = \omega^2\tau_{col}m^*/\{2cm[1 + (\omega\tau_{col})^2]\}$ (τ_{col} is the time interval between electron collisions); and $n_e(t,z) = N_e(t,z)/N_{cr}$ ($N_{cr} = \omega^2\varepsilon_0 m^*/e^2$ is the critical free-electron density).

The pump pulse envelope was approximated by a Gaussian in the numerical model. The dispersive pulse broadening was estimated approximately [10].

For convenience of comparing calculated and measured (at $p = 1$) dependences, expression (2) was written in the form

$$\Delta n(t,z) = n_2 I_1(t,z) + \frac{-n_e(t,z)f_{CB} + n_{te}(t,z)F}{2n_0}, \tag{4}$$

where

$$F = \frac{f_{tr}}{(m/m^*)(\omega_{tr}^2/\omega^2 - 1)}; \tag{5}$$

n_e and n_{te} are, respectively, the densities of free electrons and excitons, normalised to N_{cr}.

Let us assume that the charge carrier kinetics in $As_{40}S_{60}$ glass involves the same processes as the kinetics in NaCl [15]: after the charge separation due to the two-photon absorption, hole self-trapping occurs with subsequent capture of holes by electrons and formation of self-trapped excitons. The corresponding system of kinetic equations can be written as

$$\begin{aligned}
\frac{\partial n_h(t,z)}{\partial t} &= \sigma_2 I_1^2(t,z) - \frac{n_h(t,z)}{\tau_h},\\
\frac{\partial n_{th}(t,z)}{\partial t} &= \frac{n_h(t,z)}{\tau_h},\\
\frac{\partial n_e(t,z)}{\partial t} &= \sigma_2 I_1^2(t,z) - \sigma_{cr}n_e(t,z)[n_{th}(t,z) - n_{te}(t,z)],\\
\frac{\partial n_{te}(t,z)}{\partial t} &= \sigma_{cr}n_e(t,z)[n_{th}(t,z) - n_{te}(t,z)],
\end{aligned} \tag{6}$$

where n_h and n_{th} are, respectively, the densities of free and captured holes, normalised to N_{cr}; τ_h is the hole self-trapping time; $\sigma_2 = \beta_2/(2h\nu N_{cr})$; and $\sigma_{cr} = \sigma_{cap}\nu N_{cr}$ (σ_{cap} is the hole capture cross section by conduction electrons and ν is the average velocity of conduction electrons).

The system of equations (3), (6) was solved numerically with the following initial conditions: $n_h = n_{th} = n_e = n_{te} = 0$. Nonlinear coefficients n_2 and β_2 were obtained in [10]. The τ_h, σ_{cap}, and F values were chosen when analysing the numerical solution results and comparing the phase shift derived from (1) [with (4) substituted] with the curves in Fig. 2a. Since the m^* value for $As_{40}S_{60}$ is known [23] and the frequency ω_{tr} differs only slightly from the frequency $2\pi E_g/h$, the F value can be used to determine f_{tr}. The values of the parameter at which the calculated curves in Fig. 2a are in good agreement with the measurement results for Δt in the range of 0–4 ps are given below.

Kerr constant n_2/cm^2 W^{-1} . . . . . 0.8×10^{-14}
Two-photon absorption coefficient β_2/cm W^{-1} . . . . . 2×10^{-9}
One-photon absorption coefficient α_0/cm^{-1} 0.1
Self-trapping time τ_h/fs 85
Electron effective mass in the conduction band, m^* . . . . . $0.46m$
Oscillator strength for the transition to the conduction band, f_{CB} 1
Oscillator strength for the transition to the exciton band, f_{tr} 0.02
Frequency of transitions to the exciton band, ω_{tr}/rad s^{-1} . . . . . 3×10^{15}

Since the ν value is unknown for a given glass, the parameter $\sigma_{cap}\nu$ was set in the calculations. The obtained $\sigma_{cap}\nu$ value was found to depend on n_e (i.e., on energy E): $\sigma_{cap}\nu = 2.2 \times 10^{-6}$ and 5.8×10^{-6} cm^3 s^{-1} for $E = 4.1$ and 9.2 μJ, respectively.

Note that the radiation energy is transferred to a sample mainly via two-photon absorption. For example, at E = 9.2 μJ, the parameter $\beta_2 I_0 \approx 2000$ cm^{-1}, while at $E = 4.1$ μJ $\beta_2 I_0 \approx 900$ cm^{-1}. Because of the rapid decrease in intensity during pulse propagation through a sample, the probe beam phase changes (under soft-focusing conditions for the pump beam) on the front sample surface (in a surface layer with a thickness of several tens of micrometers). Since the maximum n_e value for $E = 9.2$ μJ does not exceed $0.1N_{cr}$ ($N_{cr} = 9 \times 10^{20}$ cm^{-1}), the contribution of the Joule loss at this energy leads to a small (about 1%–2%) variation in the phase shift in the minimum of the dependence $\Delta\varphi(\Delta t)$. Destruction of the sample surface was observed at $E \approx 16$ μJ ($I_0 \approx 1.6$ TW cm^{-2}).

Since the character of nonlinear response dynamics in $As_{40}S_{30}Se_{30}$ glass is the same as in the quartz sample analysed in [15], the corresponding system of kinetic equations can be written as

$$\frac{\partial n_e(t,z)}{\partial t} = \sigma_2 I_1^2(t,z) + \sigma_b n_{te}(t,z) I_1(t,z) - \frac{n_e(t,z)}{\tau_e},$$

$$\frac{\partial n_{te}(t,z)}{\partial t} = \sigma_1 I_1(t,z) - \sigma_b n_{te}(t,z) I_1(t,z) + \frac{n_e(t,z)}{\tau_e}. \quad (7)$$

Here, $\sigma_1 = \alpha_0/(h\nu N_{cr})$; $\sigma_b = \sigma_{ex}/(h\nu)$, where σ_{ex} is the one-photon absorption cross section of a self-trapped exciton; and τ_e is the transition time of conduction electrons to exciton states. In this glass, in contrast to $As_{40}S_{60}$, photoexcitation may occur via exciton band levels by means of two-step transitions at nonlinear absorption. Model (7) also takes into account the one-photon transitions to the exciton band and the transitions from the exciton band to the conduction band. However, their contributions are small, and the radiation energy is transferred to the sample mainly through two-photon (two-step) absorption. In particular, at $E = 5.1$, 2.6, and 1.7 μJ, the parameter $\beta_2 I_0 \approx 1000$, 500, and 300 cm^{-1}, respectively (the n_2 and β_2 values were obtained in [10]). The maximum n_e value for $E = 5.1$ μJ does not exceed $0.06N_{cr}$; therefore, the influence of Joule loss is weak. Destruction of the sample surface was observed at $E \approx 10$ μJ ($I_0 \approx 720$ GW cm^{-2}).

Below we report the calculated parameters for $As_{40}S_{30}Se_{30}$ glass at which the curves in Fig. 2b show good agreement with the measurement results ($\Delta t = 0$–4 ps).

Kerr constant n_2/cm^2 W^{-1} . . . . . 0.4×10^{-14}
Two-photon (two-step) absorption coefficient β_2/cm W^{-1} . . . . . 2.7×10^{-9}
Linear absorption coefficient α_0/cm^{-1} 0.4
Linear absorption cross section for exciton, σ_{ex}/cm^2 . . . . . 2.5×10^{-30}
Electron trapping time τ_e/fs 400
Electron effective mass in the conduction band, m^* . . . . . $0.46m$
Oscillator strength for the transition to the conduction band, f_{CB} 1
Oscillator strength for the transition to the exciton band, f_{tr} 0.7
Frequency of transitions to the excition band, ω_{tr}/rad s^{-1} . . . . . 2.7×10^{15}

5. Discussion

Two types of nonlinear response dynamics were revealed in glasses of the $As_{40}S_{60-x}Se_x$ system after their exposure to a 50-fs laser pulse with a wavelength of 0.79 μm. In the case of partial replacement of sulphur with selenium, the R value varied from 0.66 ($x = 0$) to 0.82 ($x = 45$).

In the $As_{40}S_{60}$ sample ($R = 0.66$), charge carriers are separated as a result of two-photon transitions from the valence band to the conduction band, and relaxation occurs through successive carrier capture with the formation of self-trapped excitons; the exciton formation time depends on the initial density of photoinduced electron–hole pairs (i.e., on the pump energy). Before the transition to the bound state, conduction electrons can move over the molecular network. Dynamics of the same type was observed in samples of compositions with $x = 15$ and 20; here, at the same pump pulse energy, excitons were formed more rapidly than in the $As_{40}S_{60}$ sample, and the delay Δt_0 was shorter at larger x values. In particular, at $E = 6$ μJ, the transition time of conduction electrons to the exciton state in the $As_{40}S_{60}$ and $As_{40}S_{45}Se_{15}$ samples was, respectively, 2.3 and 0.5 ps. At $E = 3$ μJ, this transition was not observed in the $As_{40}S_{60}$ sample on time intervals up to 100 ps, whereas in the $As_{40}S_{45}Se_{15}$ and $As_{40}S_{40}Se_{20}$ samples the transition of electrons to the exciton state occurred for 1.3 and 0.5 ps, respectively.

In the $As_{40}S_{30}Se_{30}$ sample ($R = 0.78$), one-photon transitions to the exciton band under the bottom of the conduction band become possible; correspondingly, the two-photon absorption may be a two-step process. Since the top of the valence band is filled with energy levels of lone pair electrons, in the case of absorption in the Urbach tail (or near its red

edge), an electron from a lone pair can pass, jointly with a hole, to a bound state in the exciton band. The exciton formation time is independent of E. The electron can absorb another photon and pass for some time to the conduction band and then return to the bound state at the same site of the molecular network. Dynamics of the same type was observed in samples of compositions with $x = 40$ and 45. In the sample with $x = 40$, electrons pass to the bound state for 0.5 ps, independent of E. For the sample with $x = 45$, the curves $\Delta\varphi(\Delta t)$ did not enter the domain of negative values [17]. At all E values in the range of 0.4–6.1 μJ, only positive $\Delta\varphi$ values were obtained for this sample at different Δt; this fact may indicate the absence of conduction electrons. At the same time, the Kerr peak in the dependence $\Delta\varphi(\Delta t)$ is asymmetric; this asymmetry increases with an increase in E, which may be related to the contribution of conduction electrons and their ultrafast recombination. At even higher Se content in the glass composition ($x = 60$), the probability of one-photon transition from the valence band to the conduction band increases, and the character of the nonlinear response becomes more complicated. For example, for the $As_{40}Se_{60}$ composition, instead of the Kerr peak in the dependence $\Delta\varphi(\Delta t)$ in the vicinity of $\Delta t \approx 0$, one can observe oscillations; $\Delta\varphi$ may take both positive and negative values [16].

Based on the known concepts about photoinduced chemical and structural changes in CGs [1, 2, 24–28], one can conclude that the two-photon absorption in $As_{40}Se_{60}$ leads to break of covalent interatomic bonds and formation of positively and negatively charged regions near dangling bonds (the so-called charged defects) [25–27]. As a result, the spatial orientation of covalent bonds changes, and charged defects are displaced, which changes the topology of the entire molecular network. At a high density of photoinduced conduction electrons, these changes occur more rapidly, which may be caused by stronger heating of the glass. Excitons are formed during bond rearrangement. Since partial replacement of sulphur with selenium reduces the connectivity of network sites, these photoinduced processes occur more rapidly in samples of $As_{40}S_{60-x}Se_x$ compositions with larger x (for $x < 30$).

In the case of illumination of samples with $x = 30$, 40, and 45, carrier self-trapping occurs even when one photon is absorbed; the second photon is absorbed by the self-trapped exciton. The exciton formation has no threshold with respect to the pump pulse energy, in contrast to the samples with $x = 0$, 15, and 20. An excitation of an electron from a lone pair is accompanied by a change in the interatomic potentials, which leads to the rotation of chalcogen atom and twisting of linked structural units ([$As(Ch)_3$ pyramids]) [26]. According to the model of valence-alternation pairs, the formation of a self-trapped exciton is accompanied by the occurrence of a neighbouring lone pair electrons [27, 28]. These structural changes in a molecular network site occur in a limited region, with sizes of the same order as the interatomic distances. Since the density of bound states in the band gap depends on the degree of glass purity and glass formation conditions, no significant correlation between the glass compositions with $x = 30$, 40, and 45 and the exciton formation time was experimentally observed.

6. Conclusions

Nonlinear response dynamics of two different types can be observed in glasses of the $As_{40}S_{60-x}Se_x$ system exposed to femtosecond laser pulses. The reason is that the charge carrier photoexcitation in these glasses may occur through bound states in the band gap or without their participation. If the laser pulse frequency lies far from the Urbach tail (the ratio of the pump photon energy to the bandgap energy $R < 0.78$), the carrier photoexcitation is the result of two-photon absorption; self-trapped excitons are formed by conduction electrons and self-trapped holes. In this case, the structural changes, which have a threshold with respect to the laser pulse energy, can be described within the model of charged-defect motion within the molecular glass network. If the laser pulse frequency is close to the red edge of the Urbach tail ($0.78 < R \leqslant 0.9$), self-trapped excitons are formed as a result of direct one-photon transitions of charge carriers to bound states. The structural changes, which have no threshold with respect to the laser pulse energy in this case, occur according to the valence-alternation pair type and are localised.

These conclusions are based on good agreement between the experimental data and results of computer simulation of the charge carrier kinetics and on the analysis of the known concepts about photoinduced effects in CGs. To refine the theoretical model, it is necessary to take into account the nonlinear effects leading to possible frequency conversion of laser radiation (in particular, Raman scattering).

The results of this study can be directly used to optimise the technology of waveguide structure fabrication in the bulk and on the surface of glass by the method of laser modifications.

Acknowledgements. We are grateful to N.M. Bityurin and A.V. Afanas'ev for their participation in the discussion of this paper.

This work was supported in part by the Russian Foundation for Basic Research (Grant No. 17-03-00655 A).

References

1. Popescu M.A. *Non-Crystalline Chalcogenides* (New York–Boston–Dordrecht–London–Moscow: Kluwer Acad. Publ., 2002).
2. Zakery A., Elliot S.R. *Optical Nonlinearities in Chalcogenide Glasses and their Applications* (Berlin, Heidelberg, New York: Springer-Verlag, 2007).
3. Musgraves J.D., Danto S., Richardson K., Hu J., in *Amorphous Chalcogenides, Advances and Applications*. Ed. by R.Wang (Singapore: Pan Stanford Publ., 2014) pp 203–250.
4. Misawa H., Juodkazis S. *3D Laser Microfabrication. Principles and Applications* (Weinheim: WILEY-VCH Verlag GmbH & Co. KGaA, 2006).
5. Efimov O.M., Glebov L.B., Richardson K.A., Van Stryland E., Cardinal T., Park S.H., Couzi M., Bruneel J.L. *Opt. Mater*., **17**, 379 (2001).
6. Hughes M., Yang W., Hewak D. *Appl. Phys. Lett*., **90**, 131113 (2007).
7. Romanova E.A., Konyukhov A.I., Furniss D., Seddon A.B., Benson T.M. *J. Lightwave Technol*., **27**, 3275 (2009).
8. Todorov R., Tasseva J., Bavera T., in *Photonic Crystals-Innovative Systems, Lasers and Waveguide*s. Ed. by A. Massaro (InTech, 2012) pp 143–168.
9. Blonskyi I., Kadan V., Shpotyuk O., Iovu M., Pavlov I. *Opt. Mater*., **32**, 1553 (2010).
10. Romanova E., Kuzyutkina Y., Shiryaev V., Abdel-Moneim N., Furniss D., Benson T., Seddon A., Guizard S. *J. Non-Cryst. Solids*, **480**, 13 (2018).
11. Barney E.R., Abdel-Moneim N.S., Towey J.J., Titman J., McCarthy J.E., Bookey H.T., Kar A., Furniss D., Seddon A.B. *Phys. Chem. Chem. Phys*., **17**, 6314 (2015).

12. Harbold J.M., Ilday F.O., Wise F.W. *Opt. Lett*., **27**, 119 (2002).
13. Wang T., Gai X., Wei W., Wang R., Yang Z., Shen X., Madden S., Luther-Davies B. *Opt. Mater. Express*, **4**, 1011 (2014).
14. Cardinal T., Richardson K.A., Shim H., Schulte A., Beatty R., Le Foulgoc K., Meneghini C., Viens J.F., Villeneuve A. *J. Non-Cryst. Solids*, **256&257**, 353 (1999).
15. Martin P., Guizard S., Daguzan Ph., Petite G., D'Oliveira P., Meynadier P., Perdrix M. *Phys. Rev. B*, **55**, 5799 (1997).
16. Romanova E., Chumakov K., Mouskeftaras A., Guizard S., Abdel-Moneim N., Furniss D., Seddon A.B., Benson T.M. *Proc. 15th Int. Conf. on Transparent Optical Networks (ICTON)* (Spain, Cartagena, 2013) pp 1–4.
17. Romanova E.A., Kuzyutkina Yu.S., Konyukhov A.I., Abdel-Moneim N., Seddon A.B., Benson T.M., Guizard S., Mouskeftas A. *Opt. Eng*., **53**, 071812 (2014).
18. Xuecai Han, Haizheng Tao, Ruikun Pan, Yudong Lan, Chunli Shang, Xiaoming Xing, Qianyue Tu, Xiujian Zhao. *Phys. Procedia*, **48**, 59 (2013).
19. Alekberov R.I., Mekhtiyeva S.I., Isayev A.I., Fábián M. *J. Non-Cryst. Solids*, **470**, 152 (2017).
20. Pop M.M., Shpak I.I., Kozak M.I., Semak D.G. *Fiz. Khim. Stekla*, **35**, 202 (2009).
21. Felty E.F., Lucovsky G., Myers M.B. *Solid State Commun*, **5**, 555 (1967).
22. Abdel-Moneim N. *PhD Thesis* (University of Nottingham, 2013).
23. Singh J. *J. Non-Cryst. Solids*, **299–302**, 444 (2002).
24. Musgraves J.D., Richardson K., Jain H. *Opt. Mater. Express*, **1**, 921 (2011).
25. Kolobov A.V., Tanaka K., in *Handbook of Advanced Electronic and Photonic Materials and Devices*. Ed. by H.S. Nalwa (San Diego: Acad. Press, 2001) pp 47–90.
26. Anheier N.C. Jr, Johnson B.R., Sundaram S.K., in *Non-Crystalline Materials for Optoelectronics, Optoelectronic Materials and Devices* (Bucharest: INOE Publ. House, 2004) Vol. 1, pp 259–297.
27. Kolobov A.V., Lyubin V.M., Yasuda T., Tanaka K. *Phys. Rev. B*, **55**, 23 (1997).
28. Kolobov A., Oyanagi H., Roy A., Tanaka K. *J. Non-Cryst. Solids*, **227–230**, 710 (1998).